Liquid Residence Time Distribution in the Film Flow Monolith Reactor

Achim K. Heibel
Corning Inc., Corning Environmental Technologies, Corning, NY 14831

Paul J. M. Lebens
Akzo Nobel Catalysts b.v., 1030 BE Amsterdam, The Netherlands

Jack W. Middelhoff, Freek Kapteijn, and Jacob Moulijn
Reactor and Catalysis Engineering, Delft University of Technology, 2628 BL Delft, The Netherlands

DOI 10.1002/aic.10288
Published online in Wiley InterScience (www.interscience.wiley.com).

An experimental method and data analysis procedure are introduced to determine the liquid residence time distribution (RTD) of monoliths based on the imperfect pulse injection of a dye tracer. Repeatable experiments for two different lengths allowed for the deconvolution of the RTD function of a 375-mm-long monolith section with 3.64-mm^2 channels out of dense ceramic material. The experimentally determined liquid saturations are in fair agreement with the predictions of computational fluid dynamics (CFD) calculations, assuming uniform corner flow in the square channels. The laminar film flow results in strong tailing of the RTD curves and large reduced standard deviation values. Despite the reasonable agreement for the mean residence time the CFD model based on uniform liquid distribution over the monolith channels and the individual channel corners failed to describe the experimentally determined reduced RTD curves. Applying a measured corner-scale liquid distribution pattern in combination with the CFD model resulted in good agreement with the experiments. Furthermore, this approach also improved the agreement between measurement and model for the mean residence time. *AIChE J,* 51: 122–133, 2005
Keywords: monolith reactor, residence time distribution, film flow, CFD, liquid distribution

Introduction

Monoliths are defined as unibody structures with many parallel channels. A variety of channel sizes and shapes are available and both metal and ceramic materials are used, but rarely plastics. The geometry of monoliths is usually described by the number of channels per cross-sectional area [cells per square inch (cpsi)] and the wall thickness separating the channels. The size of the channels may vary from 0.5 to 10 mm. Usually the catalyst is embedded in a thin washcoat layer of a high surface area material deposited on an inert and mechanically strong backbone. Monolithic structures are widely used as catalyst support in gas-phase applications because of the favorable balance between a high surface area to volume (S/V) ratio, short diffusional length, and a low pressure drop. Furthermore, they possess a very good mechanical integrity. Major areas of application are in the exhaust after-treatment of combustion engines and in the treatment of off-gases of stationary sources.[1,2]

During recent years the application of monoliths has been

Correspondence concerning this article should be addressed to A. K. Heibel at heibelak@corning.com

extended to multiphase operations.[3] The research is mostly focused on two different flow regimes, bubble-train or Taylor flow and film flow.

In Taylor flow gas bubbles separated by liquid plugs pass through the individual channels of the monolith.[4] Frequently, the reactor is operated in a cocurrent downflow mode, although investigations in upflow mode were also performed.[5] Various reactions have been investigated and proved that Taylor flow monoliths are a viable option for the replacement of slurry[6-8] and trickle-bed reactors.[9,10]

Pioneering work in the area of monoliths operated under film flow conditions was performed by Lebens et al.[11,12] The gas occupies the center of the channel and the liquid flows down the wall as a more or less stable film. The separated passages of gas and liquid allow cocurrent as well as countercurrent operation. The monolith film flow reactor is suited for applications with high single-pass conversions. In countercurrent operation stripping of inhibiting reaction products[13,14]] or overcoming thermodynamic limitations can boost the reactor performance.[15,16]

In multiphase reactors the underlying hydrodynamics have a significant impact on heat and mass transfer performances. These factors will also influence the reactive performance.[17,18] Especially for complex geometries and systems (such as multiphase reactors) it is very difficult to gain a fundamental understanding of the flow phenomena inside the reactor.[19] The residence time distribution (RTD) is a tool frequently used to understand and quantify the actual flow phenomena in chemical reactors. Significant work has been performed around the RTD behavior of trickle beds[20-23] and, more recently, for structured packings.[24-26]

The residence time distribution for monoliths in various flow regimes was previously investigated. The majority of the work concentrated on the upflow bubble-train flow regime for single round and square capillaries as well as monoliths.[27-29] The measured residence time distribution in single capillaries was successfully described with fundamental flow models, although large deviations were found for monoliths.[28] These differences were mostly attributed to the gas/liquid distribution over the various channels in a monolith. Furthermore, assumptions concerning the behavior of the in- and outlet sections had to be made for the deconvolution process,[27] which exert an impact on the obtained RTD of the monolith segment. For both single capillary and monolith measurements a large amount of back mixing was found, dependent on the applied flow conditions.

Lebens[11] performed the first RTD experiments for monoliths operated in the film-flow regime. The reduced RTD curves were clearly independent of the liquid velocity. Comparisons to a fundamental hydrodynamic convection model showed good agreement with the prediction of the tail of the curves, although resulting in differences for the front end of the RTD curves. Earlier breakthroughs were measured than predicted by the model and the peak value of the measured curves was significantly lower. The differences were mostly attributed to interfacial waves on the falling liquid film.

For the targeted applications of the monolith film flow reactor the gas phase reaction components are usually in stoichiometric excess. Additionally, in combination with the significantly higher diffusivities compared to those of the liquid, the flow behavior of the gas phase is of less interest compared to the liquid phase. Moreover, the residence time distribution of the liquid phase is strongly influenced by capillary, bypassing, and maldistribution effects, which might have a significant impact on the flow behavior. Therefore, in the context of this work, we concentrate on the liquid RTD in the monolith film-flow reactor.

In the context of this work we apply fundamental flow as well as diffusion models to determine the theoretical RTD based on certain assumptions for the gas–liquid phase distribution in the individual monolith channel. An experimental setup and methodology are introduced to evaluate the liquid RTD for monoliths operated in the film-flow regime. A procedure to deconvolute the results for the monolith section itself is established and applied. The results from a series of experiments for different liquid velocities are analyzed and interpreted. In the last step the deconvoluted results are compared to the model predictions and differences are analyzed and potential reasons are elucidated. Based on these findings the model is adjusted to include liquid maldistribution and, finally, the predictions of the model for typical distribution patterns are again compared to the experimental results.

Theory

RTD is a powerful concept to characterize the mixing phenomena and flow behavior in chemical reactor system, which allows comparison with ideal reactors. The time it takes for a fluid element to flow through a reactor system is called the *residence time*. The frequency density when these elements leave the reactor system after a certain residence time is expressed as the *RTD function*. The RTD is obtained by tracer tests. A disturbance is given to the inlet of the system by means of a tracer injection and the response of the system is measured through the tracer concentration at the exit of the system. The way the dynamic disturbance (that is, tracer injection) is transformed characterizes the mixing patterns and flow characteristics within the reactor system.

For a perfect pulse disturbance the RTD can be expressed by means of the distribution function evaluated from the tracer response at the exit of the reactor or the reduced distribution function normalized by the mean residence time

$$E_t = \frac{c_e(t)}{\int_0^\infty c_e(t)dt} \qquad E_\theta = E_t\tau \tag{1}$$

The cumulative distribution curves result from integration

$$F_t = \int_0^t E_t dt \qquad F_\theta = \int_0^\theta E_\theta d\theta \tag{2}$$

The mean residence time

$$\tau = \int_0^\infty tE_t dt \tag{3}$$

and the variance of the residence time distribution around its mean

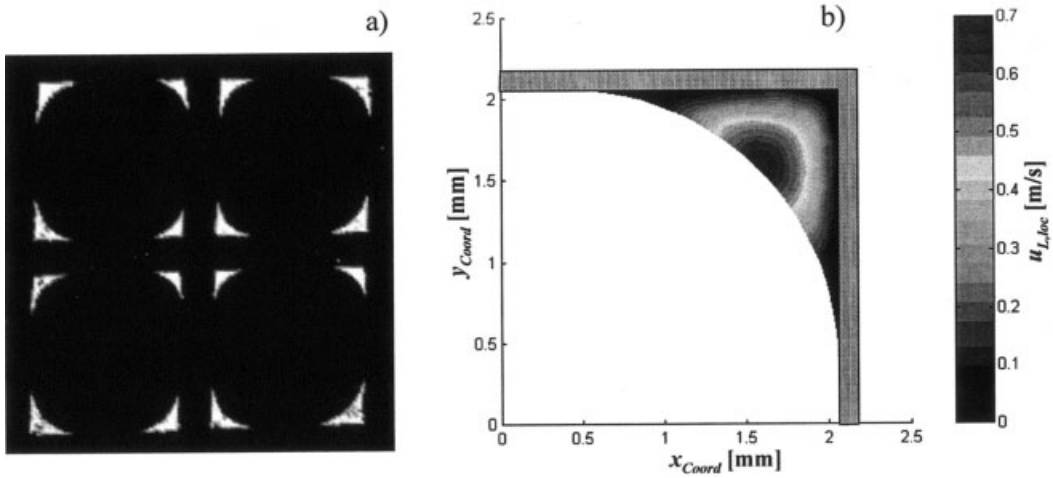

Figure 1. (a) Magnetic resonance image of liquid flowing through four square monolith channels, d_h = 4.12 mm, u_{Ls} = 2.2 cm/s: (b) velocity field in one corner of a square channel as calculated by the hydrodynamic model (Eq. 6), d_h = 4.12 mm, u_{Ls} = 4.0 cm/s, β_L = 14%, patterned area represents channel wall.

$$\sigma_t^2 = \int_0^\infty (t - \tau)^2 E_t dt \tag{4}$$

are important characteristic parameters describing the RTD. Another very useful measure is the reduced variance

$$\sigma_\theta^2 = \frac{\sigma_t^2}{\tau^2} \tag{5}$$

which normalizes the variance by the mean residence time and therefore becomes nondimensional.

Previous research[30] concluded that the flow in the small monolith channels is laminar ($Re_L < 100$), even though disturbances on the gas–liquid interface can occur. The RTD in laminar flow is mainly determined by two fundamental phenomena: convection and diffusion. The importance and interplay of these two factors are dependent on the geometric configurations, the flow conditions, and the physical properties of the fluids. Therefore various models are useful to describe the RTD under different conditions.[17] Lebens[11] showed that for the film-flow monolith reactor the convection model and the axial dispersion model are applicable. In the context of this work, both the convection model and a convection–diffusion model are applied.

Convection model

The convection model describes the RTD based solely on the velocity field. There is no exchange (diffusion) between different streamlines. Previously, the gas–liquid distribution has been determined and a finite-element model (FEM) to describe the flow field (Figure 1) was established[31] based on the Navier–Stokes equation:

$$\nabla \cdot (\eta_L \nabla u_{L,z}) = g\rho_L \tag{6}$$

In agreement with the experiments, water was used as liquid phase and no forced gas flow was applied for the model calculations. For atmospheric pressure (1.015 bar) and at room temperature (20°C) a density of 998 kg/m^3 and a dynamic viscosity of 1.0×10^{-3} Pa·s were assumed.[32]

An important aspect for the calculation of the RTD in laminar flow is the application of the correct boundary conditions.[17] In the case of planar boundary conditions the tracer is assumed to be introduced and detected equally over the cross section of the flow field. For flux boundary conditions the tracer input and collection are proportional to the local velocity.

Equation 6 was solved for the liquid domains, as described in Figure 1, using a commercial FEM package.[33] In general the RTD with flux boundary conditions can be well described by a single curve (Figure 2a) over a wide range of superficial channel velocities. The data include partial (Figure 1) as well as full irrigation of the channel walls.

For the planar boundary conditions the high velocities remote from the wall have a smaller contribution to the RTD, although the flow contribution from these areas is substantial. This leads to a lower peak value of the reduced distribution curve and higher values for the tail section (Figure 2b), representing the flow close to the walls. The correct exit age distribution is the one obtained for flux in- and outlet boundary conditions, which represents a mixing-cup measurement.[17] Here the various liquid fractions are included based on their flow contribution. As expected, both models predict the same breakthrough time.

The reduced distribution function for the flux boundary conditions can be sufficiently fitted by

$$E_\theta = -\frac{0.03}{\theta^2} + \frac{0.3}{\theta^{2.5}} + \frac{0.12}{\theta^3} \qquad \text{for } \theta \geq \frac{1}{2.375} \tag{7}$$

and

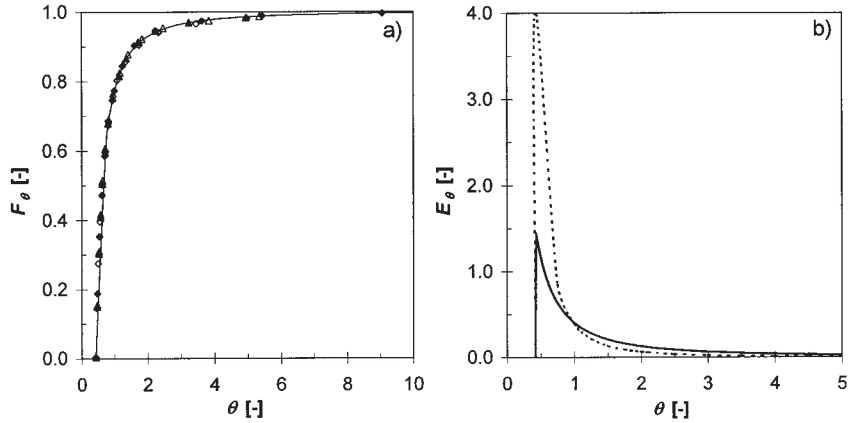

Figure 2. Results of the convection model calculations.

(a) Characteristic reduced cumulative distribution curve (flux boundary condition) for various flow conditions and liquid domains (closed symbols: partial wetting; open symbols: full wetting); line represents best fit according to Eq. 7. (b) Reduced residence time distribution curve for planar (solid line) and flux (dotted line) boundary conditions.

$$F_\theta = \frac{0.03}{\theta} - \frac{0.2}{\theta^{1.5}} - \frac{0.06}{\theta^2} + 1 \qquad \text{for } \theta \geq \frac{1}{2.375} \tag{8}$$

for the reduced cumulative distribution function.

Convection–diffusion model

In this case, besides the flow field (Eq. 6), the mass balance for the tracer[31] is also solved

$$\frac{\partial c}{\partial t} + u_{L,z}\frac{\partial c}{\partial z} = \nabla \cdot (D \nabla c) \tag{9}$$

and therefore diffusion effects are included. A diffusivity of 2.0×10^{-9} m^2/s for the tracer in water was assumed for the calculations. As an initial condition the tracer concentration is set to zero in the liquid domain. For times greater than the starting time of the tracer introduction the concentration of the tracer at the liquid inlet was set to one. For the other boundaries of the liquid domain zero-flux boundary conditions for the tracer were applied. The simulations were performed using a commercial CFD software package.[34] Mesh as well as time-step independence for the calculations were checked to ensure meaningful results.

The results for the calculations with a length of 375 mm, according to the deconvoluted test section length for the experiments, are summarized in Figure 3. Different liquid superficial channel velocities were applied to gain a better understanding of the interaction between convection and diffusion phenomena. The convection models showed very similar reduced distribution curves (Figure 2a) and therefore flow behavior over a wide range of liquid superficial velocities. Indeed for higher liquid superficial velocities the reduced distribution curves of the convection–diffusion model converge and approach the behavior of the convection model. The small differences between the convection–diffusion and the pure convection model indicate the dominating effect of the convective flow compared to the lateral diffusion. A somewhat different behavior is determined for lower liquid superficial velocities (Figure 3b). Here the diffusion phenomena perpendicular to the

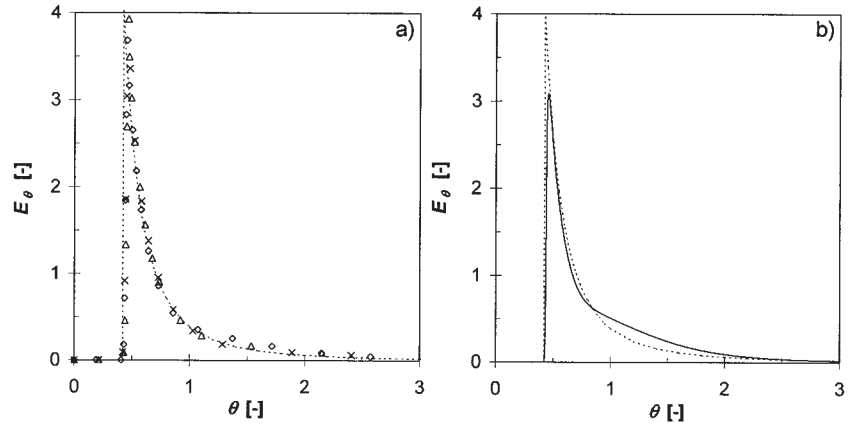

Figure 3. Reduced RTD curve results of the convection–diffusion model calculations for superficial liquid channel velocities (u_{LS}).

(a) △ 1.0 cm/s, ◇ 2.0 cm/s, × 4.0 cm/s; (b) 0.5 cm/s (solid line); dotted line represents the result for the pure convection model. Flux boundary conditions.

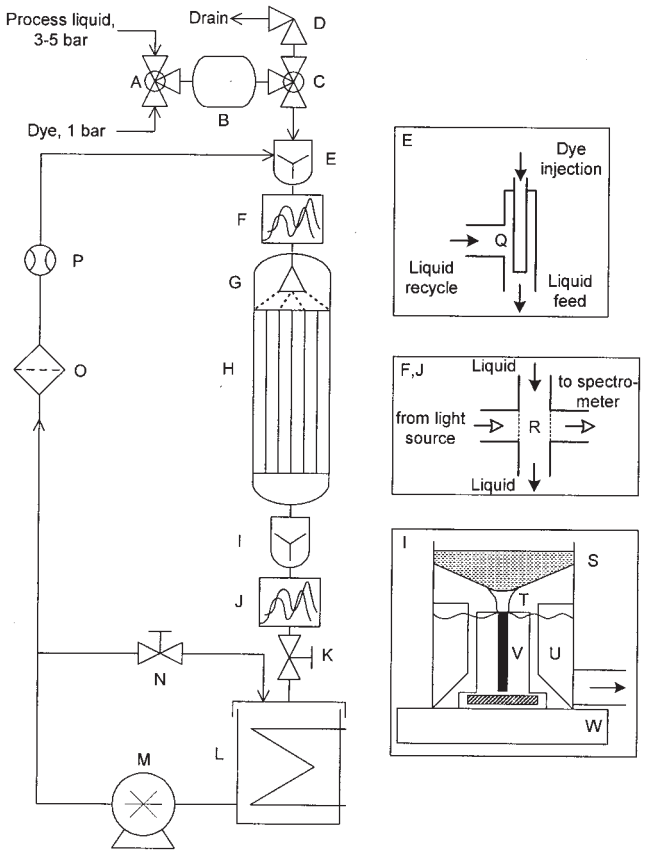

Figure 4. Experimental setup.

A: filling valve; B: dye injection volume; C: injection valve; D: drain valve; E: dye mixing section; F: inlet detection cell; G: liquid distribution section; H: monolith test section; I: collection section; J: outlet detection cell; K: liquid level valve; L: liquid tank; M: pump; N: recycle valve; O: strainer; P: flow meter; Q: dye injection pipe; R: optical path with filters; S: collection foam; T: liquid jet; U: baffles; V: magnetic stirrer; W: magnetic stirrer drive.

flow become more important. This leads to a lower maximum tracer response, attributed to the spread over the liquid-filled corner, which is then released at later times and therefore follows in more tailing. These effects will be pronounced for longer length and higher *S*/*V* ratio monoliths.

In general earlier and less-abrupt breakthroughs are found with the convection–diffusion model compared to the convection model, given the axial and lateral diffusion phenomena included in the model.

Experimental

Setup and materials

The RTD experiments were performed using imperfect pulse response experiments with a dye tracer. A schematic of the experimental setup is illustrated in Figure 4.

The liquid (tap water) was pumped with a screw pump (Monopumps, Ltd.) in a recycle to the main liquid vessel. With a valve in the recycle a controlled part of the recycled flow was directed to a filter. After passing through the filter the liquid flow was measured by a turbine flow sensor (Digi-flow, DFS 2, ±1% full scale). The tracer was applied by a special valve system to ensure the consistent injection of a fixed amount of tracer. To achieve this a prefilled dye injection volume was injected with process liquid using a fast-response valve (Bürkert, ±15 ms). It was determined that the maximum impact of the injected volume flow on the liquid flow rate was less than 10% for the lowest applied liquid flow rate.

A custom-made injection fitting was designed to allow for good mixing of dye (Ecoline® solution of 0.35 wt %) and process liquid (Figure 4, part E). Before entering the nozzle the liquid flow was monitored for the dye concentration with an optical flow cell (Ocean Optics Inc.). The optical flow cells are crosslike structures with a perpendicular light and liquid pass (Figure 4, parts F and J). The light passes through a set of optical filters and is absorbed by the liquid as a function of the dye concentration. After that optical fibers guide the light to a microspectrometer (Ocean Optics, Inc.) detecting the intensity for a wavelength scan.

Two different nozzles (FullJet, Spraying Systems, Inc.), covering the flow range of interest, distributed the liquid evenly over the monolith cross section. Before the RTD experiments the appropriate nozzle positioning was determined by cold-flow testing in a special cold-flow distribution setup.[31]

The liquid passed the channels of the monolith and was collected with a small stirred vessel with baffles (mixing cup) after passing through a ceramic foam for gas–liquid separation and formation of a single liquid jet flowing smoothly on the top of the stirrer in the collection vessel (Figure 4, part I). The liquid level in the mixing cup was closely monitored to ensure a fixed residence time required for comparing the different experiments. From the mixing cup the liquid was led through another optical flow cell (Ocean Optics Inc.), in which the concentration of the dye was measured, before running back into the main liquid vessel.

The experimental setup was fully automated, including the injection system, and all data were acquired with a frequency of approximately 25 Hz. All experiments were performed at room temperature and ambient pressure.

The custom-made dense monoliths (Corning Inc.) had a diameter of 0.043 m and two different lengths of 125 and 500 mm were investigated. Monoliths of 34 cpsi, with square channels of a hydraulic diameter of 3.64 mm, were used for the experiments. Monoliths of dense cordierite ($2MgO{\cdot}2Al_2O_3{\cdot}5SiO_2$) were used for the studies to eliminate any effects of tracer diffusing in and out of a porous structure. The monoliths were mounted in special PVC tubes with flanges to connect the custom-made distribution and collection section. The partial channels around the boundary of the monoliths were blocked with a two-component glue to obtain a defined geometry of 64 square channels.

Procedures and data analysis

Before the experiments the optical system was calibrated with dye solutions of known concentrations and the relationship between concentration and absorbance according to the Lambert–Beer law was established. Furthermore, a reference signal of the process water was measured before each dye injection. The concentration was then determined according to the following equation

$$c = k_{\lambda,s}\ln\left(\frac{I_{meas} - I_{dark}}{I_{ref} - I_{dark}}\right) \tag{10}$$

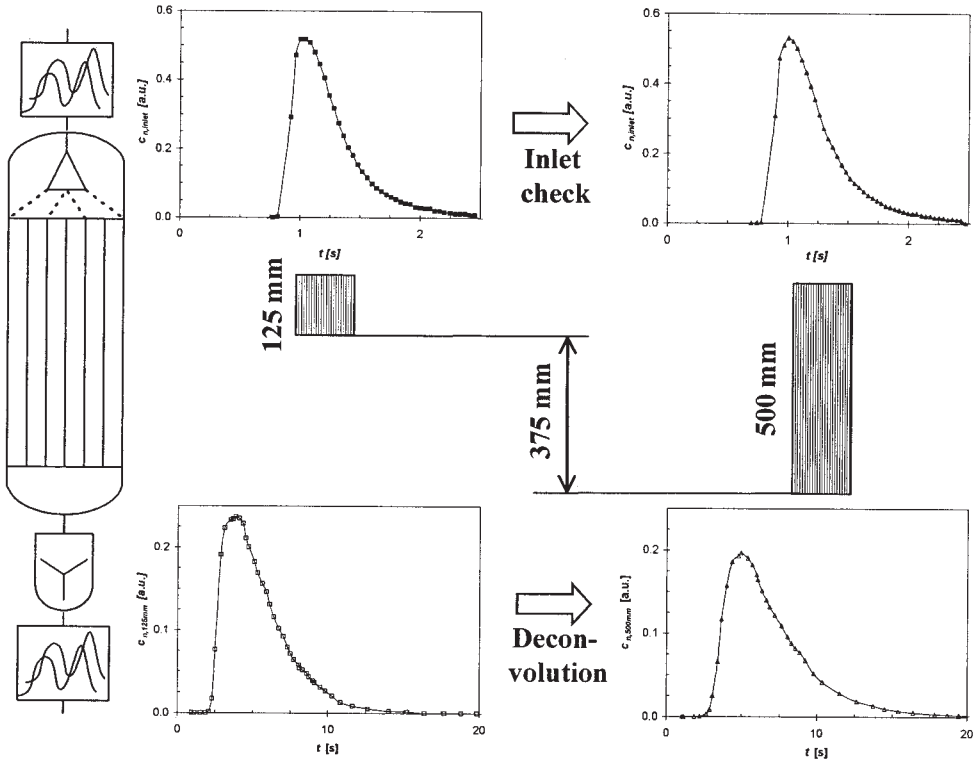

Figure 5. Data processing scheme.

Measurement of two different monolith lengths at a given flow rate using the same distribution and collection section, check of the inlet pulse ensuring similar measurement conditions, and deconvolution of the monolith tracer response from the two outlet signals.

Some entrapment of gas was observed in the liquid flowing through the optical cell at the outlet. These small gas bubbles had a significant impact on the absorption/scattering of the light. Therefore the signal was conditioned using an envelope technique, filtering out the data points for the high absorption gas bubble measurements.[35] Furthermore, for the low concentrations representing mostly the tail of the time series measured at the outlet a filter was applied to improve the signal-to-noise ratio.[36]

The analysis was executed according to the scheme represented in Figure 5.

All experiments were repeated five times and showed very good agreement (Figure 6a) between them. Therefore one run was used as a representative for the specific condition for further analysis. RTD experiments for the short and long monoliths were performed with the same distribution and collection section and the related time series measured at the exit were synchronized using the signal before the inlet of the test section. Based on the differences in the opening of the injection valve, only small time shifts were required (<250 ms) and generally the injection pulses were remarkably reproducible (injected amount of tracer as well as shape of the inlet pulse).

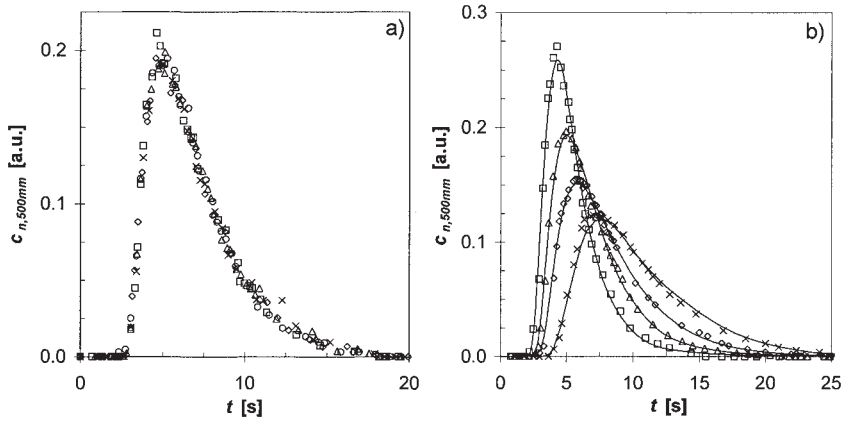

Figure 6. Tracer response curves at the outlet of the monolith.

(a) Repeatibility for five different experiments, u_{Ls} = 2.6 cm/s. (b) Experimental data for superficial liquid channel velocities (u_{Ls}) (in cm/s) of □ 3.9, △ 2.6, ◇ 2.0, and × 1.5; lines represent optimized results of the deconvolution model for the different velocity conditions.

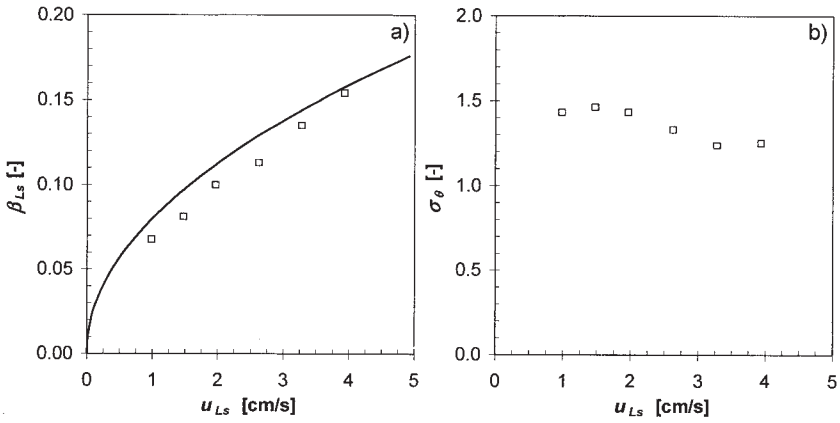

Figure 7. (a) Liquid saturation as a function of superficial liquid channel velocity; line represents convection model predictions;[38] (b) standard deviation of the reduced RTD curves as a function of superficial channel velocity.

Finally, the RTD of the monolith section itself, without the effects from the liquid distribution and collection section, was determined by deconvolution from the exit traces of the short and long monolith experiments. The deconvolution was performed in the time domain using a two-variable one- dimensional model.[37] This model is composed of piston flow with axial dispersion and mass transfer with a stationary phase (piston–diffusion–exchange model). An optimization of several fitting parameters was performed to minimize the deviation between model data at the outlet and the experimental data (Figure 6b). A finite-element solver (Comsol AB, Femlab[33]) with an optimization routine (Matlab, The MathWorks, Natick, MA) was used to solve the problem numerically.

Finally, the cumulative distribution function was determined by a step-response calculation using the model with the optimized fitting parameters for a given flow condition. The reduced distribution curve followed simply by taking the derivative and normalization.

Results and Discussion

Experimental results

As described earlier the residence time distribution is frequently described by the mean residence time (Eq. 3) and the variance (Eq. 4). The experimental results for the short and the long monolith allow determination of the mean residence time of the differential monolith section and therefore the calculation of the liquid saturation

$$\beta_{Ls} = \frac{(\tau_{long} - \tau_{short})u_{Ls}}{(l_{long} - l_{short})} \tag{11}$$

The reduced standard deviation of the distribution curve is determined[17]

$$\sigma_\theta = \sqrt{\frac{\sigma^2_{long} - \sigma^2_{short}}{(\tau_{long} - \tau_{short})^2}} \tag{12}$$

Both variables are illustrated in Figure 7 as a function of the superficial liquid channel velocity.

In agreement with the expectations larger liquid saturations are found for increasing liquid flows. The same trend is calculated using the convection model, although the experimental values are generally lower (10–15%) than the calculated values. Previous investigations[31,38] showed excellent agreement between the liquid saturation calculated by the convection model and experimental results from MRI measurements of the four channels in the center of the monolith. With a proper positioning of the liquid distributor the flow in the four center channels is generally very close to the expected value for a uniform distribution. In the context of this work all the channels contribute to the overall residence time distribution and therefore maldistribution effects over the channels are included. Because of the decreasing slope of the saturation with increasing liquid velocity, maldistribution effects will lead to an overall lower value of the liquid saturation compared to that of the uniform distribution case.[30,31] Therefore nonuniform liquid distribution might explain the lower liquid saturation values determined in the experiments. Another possible phenomenon leading to lower liquid saturation than that determined by the convection model might be the formation of fast-traveling waves at the gas–liquid interface.[30]

The reduced standard deviation is a good measure of the relative width of the residence time distribution curve attributed to the normalization with the mean residence time. Values larger than one are common for laminar flow–dominated systems.[36] This indicates the strong tailing of the residence time distribution curves, resulting from the nearly zero-velocity fluid elements near the wall and the limited exchange with the faster flowing fluid elements. The measurements show a slight decrease of the reduced standard deviation with increasing liquid velocity, which is in good agreement with the trend previously reported by Lebens.[11] The trend might be explained by wave formation at higher flow rates, which will lead to increased plug flow behavior. Furthermore, the liquid distribution measurements indicated somewhat less uniform distribution for lower flow rates,[38,39] which will lead to a larger variance value in the residence time distribution.

In Figure 6b the application of the numerical deconvolution method for various flow conditions was illustrated and discussed. The distribution curves obtained according to the deconvolution are summarized in Figure 8a.

As expected, the peak of the curve moves to higher values

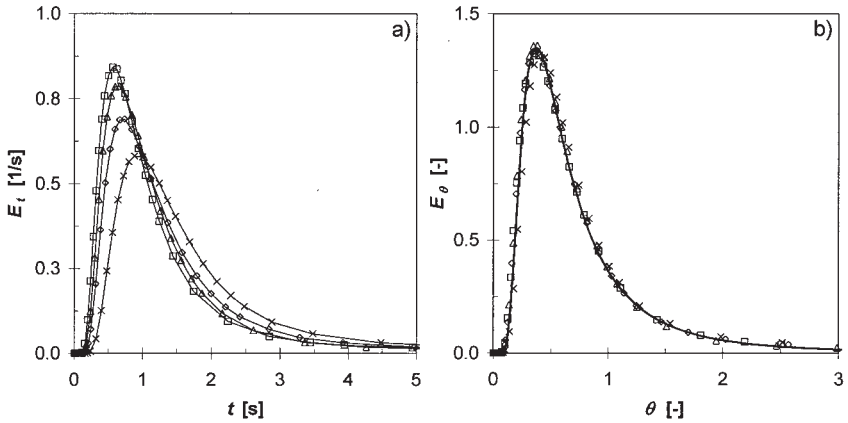

Figure 8. (a) Deconvoluted RTD curves and (b) reduced RTD curves for different superficial liquid channel velocities (u_{Ls}) (in cm/s) of □ 3.9, △ 2.6, ◇ 2.0, and × 1.5; line in (b) represents Eq. 13.

and shorter times with increasing velocity. Also a strong tailing of the RTD is apparent.

In a second step the reduced residence time distribution functions have been determined by normalizing with the mean residence time (Figure 8b). The data for the various flow conditions under investigation coincide well. Indeed it is found that the reduced RTD curve is independent of the superficial channel velocity. Common characteristics for the reduced RTD of the different velocities are the rather short and abrupt breakthrough times, the low peak values, and the long tails. The tail of the RTD converges to zero for large reduced residence times. The rather abrupt breakthrough behavior is a result of the strong convective behavior of the system, where smoothing effects attributed to dispersion are secondary. The long tail of the curve is a result of the underlying laminar film flow hydrodynamics with the very limited exchange perpendicular to the main flow direction. However, for very large reduced residence times the RTD curve approaches zero, which is not expected for a purely convective system. In this case the rather slow molecular diffusion effects help to decay the tracer signal by exchange perpendicular to the main flow direction. According to Levenspiel,[40] the Bodenstein number ($Bo_{lat} = ud_{char}/D$) and the ratio of reactor length to characteristic length dimension (l/d_{char}) can be used to understand the flow behavior of a system. To compare the film-flow monolith reactor to the more common pipe-flow systems described in the literature, the average film thickness is used as half of the characteristic length dimension. For the current experimental conditions we find Bodenstein (Bo) numbers in the range of 2.0×10^4 to 5.0×10^4 and the ratio of reactor length to the characteristic length dimension (l/d_{char}) ranges from 0.85×10^3 to 1.35×10^3. The high Bodenstein numbers result from the strong convective flow contributions in the liquid film. Based on the dimensional groups identified for this study, Levenspiel[40] recommends the application of a pure convection model to describe the flow behavior of the system.

A good description of all the reduced distribution curves is obtained by applying a nonlinear fit function (inverted-gamma function),[41] which is also presented in Figure 8b

$$E_\theta = 4.7(3.7\theta + 0.03)^{-3.7} e^{[(\theta-0.37)13.7]/(3.7\theta+0.03)} \qquad (13)$$

It is important to note that Eq. 13 describes only the results of the current work and caution is required to extrapolate outside the experimental space of this study. All the experiments in the context of this work were performed in the partial irrigation regime (Figure 1), where the corner-flow phenomena are dominating. The mean residence time used to calculate the reduced time can also be determined as a function of the channel geometry and liquid viscosity and density, as previously experimentally and analytically shown for a variety of liquid systems.[30,42] Liquids with different surface tensions as well as operation in the total irrigation regime might lead to a different flow behavior, especially concerning the stability of the liquid film and therefore potential wave formation. This might result in a different residence time behavior, especially on the front end of the RTD. With the current description we find an exponential decay for large residence times. As mentioned above, this behavior cannot be explained by a pure convection model for laminar film-flow systems, although it is commonly experienced in real laminar systems as the diffusion in the liquid film becomes important for larger residence times (see also results from convection–diffusion model; Figure 3).[36,37]

Previously, Lebens[11] performed residence time distribution measurements in an internally finned monolith under similar flow conditions, using an imperfect salt-tracer pulse-injection method with conductivity measurements at the outlet. A different experimental setup was used including the liquid distribution devices and the collection section of the bottom of the monolith. Furthermore, the tracer was measured directly in the collection vessel. The channel shape and *S/V* ratio of the monoliths were quite different. For the sake of comparison the deconvoluted data of Lebens[11] for a 500-mm-long monolith is shown in Figure 9 with the current results.

Good agreement is found for the reduced distribution curves determined by Lebens and the current work. This indicates that, despite the geometric differences for the two monoliths studied, the underlying flow phenomena are rather similar. Indeed it is assumed that in both cases laminar film flow in the corners of the channels is leading to a dominating convective contribution in the RTD. For the finned monoliths the number of corners per unit cross-sectional area is larger compared to that of the regular square monolith. Therefore normalization with

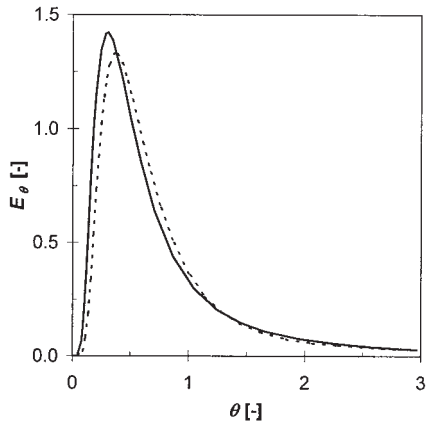

Figure 9. Comparison of the experimentally determined average reduced RTD function (dashed line) with the experimental results of Lebens[11] for a finned monolith (solid line).

the mean residence time should lead to similar pulse-response behavior.

Comparison between model and experimental results

In the theory section two models to describe the flow in the monolith channels have been introduced. For further discussions the focus will be on the convection–diffusion model for high velocities, which approaches those of the pure convection model. In Figure 10 the experimentally determined average RTD curve (Eq. 13) is compared with the model prediction.

Obviously the model and experimental results deviate significantly. The model prediction shows a significantly higher peak value and a much later breakthrough. Interestingly, the tails ($\theta > 1$) of both curves correspond strikingly well, indicating that the flow behavior of the slow-moving liquid contributions and their exchange with the fast-moving ones is described rather well with the convection–diffusion model.

The differences at the front end of the residence time distribution curve indicate that a significant amount of liquid is leaving the monolith faster than expected. The maximum velocities are about four to five times higher than predicted by the model.

These deviations can be mainly attributed to two different phenomena:

(1) Instabilities at the gas–liquid interface (interfacial waves)

(2) Liquid maldistribution effects

Interfacial waves are a common phenomena of falling films.[43] Typically it is differentiated between high frequency ripple waves on the film surface on the one hand, and strong disturbing roll waves on the other hand. Ripple waves are found under all flow conditions and are small in amplitude and insignificantly faster in velocity compared to the underlying film. Roll waves, however, flow with a rather high velocity as a separate entity over the main film in low frequencies. These large disturbances could explain the large amount of liquid leaving the monolith earlier than estimated. Visualization experiments performed by Lebens[11] indicated the occurrence of roll waves. On the other hand, previously performed MRI experiments on four isolated monolith channels resulted[38,39] in rather stable and reproducible flow conditions, which might be also attributable to the averaging based on the rather long measurement period. In any case, at this point and time, the occurrence of interfacial waves cannot be excluded, although the limited information available does not allow for a proper physical description.

A significant amount of work has been performed to understand liquid maldistribution effects in monoliths. Previous investigations[31,38,39] on monoliths operated in the film-flow regime indicated two kinds of maldistribution phenomena. On the one hand, the liquid can be unevenly distributed over the various channels of the monolith and, on the other hand, distribution differences in the individual channel can occur, which are represented by different local liquid hold-ups in the channel corners (Figure 1). Investigations[44-47] have been performed on the displacement of liquid in square channels by a gas phase. In these cases rather uniform and symmetric phase distributions were found over the cross section of the channel, as a result of the connected liquid phase being displaced. In the case of the gravity-driven liquid flow the behavior is quite different, attributed to the rather separated flow in the individual channel corners. This is especially the case in the context of this work because of the partial irrigation of the channel walls (Figure 1). Channel-scale nonuniformities may result from variations introduced by the distributor as well as geometric differences.

To include maldistribution effects two typical measured flow patterns over the monolith channels are combined with the flow deviations determined by MRI measurements over the corners of a set of four channels in the center of the monolith. This resulted in a total of 176 local superficial corner velocities based on a quarter of the open channel area. Both experiments were performed with a 25 cpsi porous cordierite monolith, with a channel size of 4.12 mm. As mentioned in the experimental section all nozzles as well as their positioning were qualified by liquid distribution tests and from the results of these tests bad distribution patterns were identified. Therefore the two selected distribution patterns over the monolith cross section resemble a good and a medium liquid distribution quality, which are representative for the distributions expected for the RTD measurements. The results are presented by the cumulative liquid

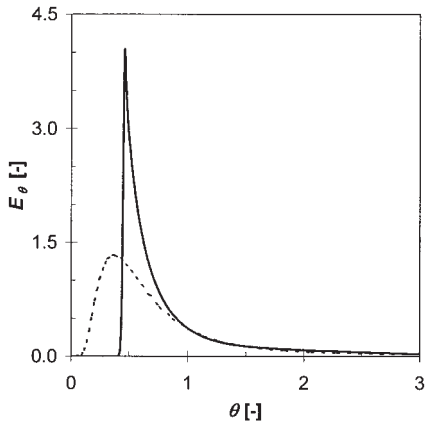

Figure 10. Comparison of the experimentally determined average reduced RTD curve (dashed line) with the results of the convection–diffusion model, u_{Ls} = 4.0 cm/s (solid line).

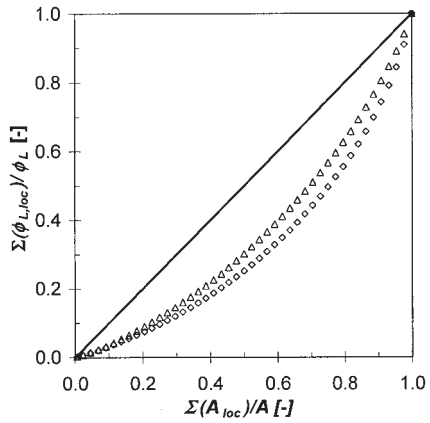

Figure 11. Liquid maldistribution represented as the relative cumulative liquid flow over the relative cumulative cross-sectional area for a medium (◇) and a good (△) liquid distribution quality; line represents uniform distribution.

flow function over the cumulative cross-sectional area (Figure 11). For a uniform liquid distribution any fraction of the cross-sectional area would be associated with the same fraction of liquid flow (see unity line). As illustrated, local velocities are lower than the average, leading to proportionally more liquid flowing through a smaller fraction of the cross-sectional area. As expected, the medium distribution quality deviates even more from the ideal case.

In a second step based on the local liquid velocities the mean residence time was determined based on the results of the convection model for a single corner (Eq. 6). The results based on this analysis show good agreement between model predictions, including maldistribution effects and the experimental data (Figure 12a). In general, because of the maldistribution lower liquid saturation values are found (compare Figure 7a), with a more pronounced effect for the medium liquid distribution quality.

The mean residence time of the liquid in the individual corner was determined and by the reduced residence time distribution curve from the convection–diffusion model (Figure 10) the RTD curve was calculated. The RTD functions for the different corners were weighted by their velocity contribution and afterward cumulated over time to obtain the overall cumulative distribution function. Finally, normalization and derivation lead to the overall RTD curve for the given representative distribution pattern (Figure 12b).

The agreement between the prediction based on the fundamental convection–diffusion model combined with the measured distribution pattern and the experimentally determined reduced RTD curve is striking. For both distribution qualities, the calculations show a significant shift to an earlier breakthrough and a lower peak value compared to the simulations under uniform flow (Figure 10). In any case a rather similar tail of the reduced RTD curve is found, which is related to the contribution of the slow-flowing liquid near the monolith wall.

Deviations in the front end of the reduced RTD curves might be related to the differences in the monolith geometry and distributors used for the RTD compared to the liquid distribution measurements. This is also apparent from the sensitivity of the shape of the RTD curve on the distribution quality. Furthermore, these differences may be also the result of other effects such as interfacial waves in addition to the liquid maldistribution.

Conclusions

An imperfect-pulse method with a dye tracer was successfully applied to determine the liquid residence time distribution in a film-flow monolith reactor. Careful consideration of the important details—such as the defined injection of a tracer volume, the collection and mixing of the liquid leaving the monolith, the application of strict experimental procedures, and the proper processing of the raw experimental data—resulted in highly reproducible and meaningful results. The measurement of two different monolith lengths allowed the deconvolution of the RTD function of the monolith section itself, without any major impact of the liquid distribution and collection section. The deconvolution was performed in the time domain using a

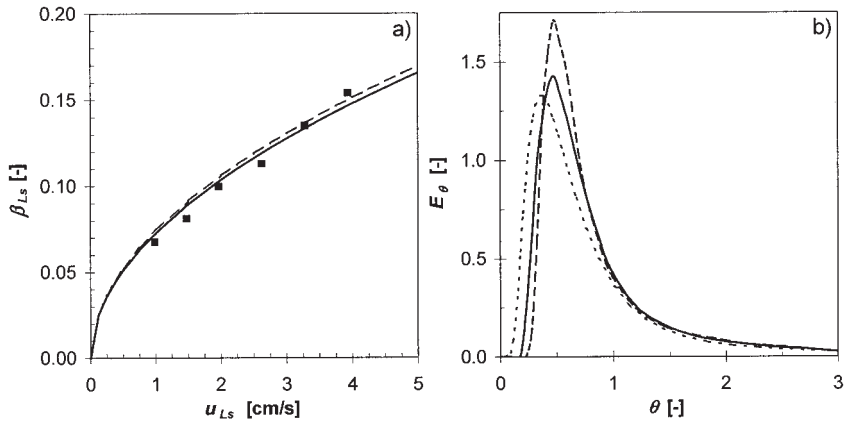

Figure 12. Impact of liquid distribution quality on (a) liquid saturation as a function of superficial channel velocity for a medium (solid line) and a good (dashed line) distribution quality; markers represent experimental data; (b) comparison of the experimentally determined average reduced distribution function (dotted line) with the convection–diffusion model (u_{Ls} = 4.0 cm/s) for a medium (solid line) and a good liquid distribution quality (dashed line).

two-variable partial differential equation model coupled with a parameter optimization.

A convective model based on computational fluid dynamics (CFD) calculations of the flow field in an individual corner of the channel resulted in a unique reduced residence time distribution function independent of flow rate. The more complex convection–diffusion model differs for lower velocities from the pure convection model resulting from the lateral diffusion over the film. For higher velocities both models converge.

A nonporous (dense) cordierite monolith, with 3.64-mm^2 channels and a deconvoluted length of 375 mm, was used in the experiments. Experimentally determined mean residence times are very similar to the predictions by the convection model, assuming a uniform flow distribution over all the channel corners. Considering liquid maldistribution the differences between model results and experiments are further reduced.

The reduced residence time distribution curves over the investigated flow range are very similar and can be described by a single function (Eq. 13) for partial irrigation of the channel walls (Figure 1). The results are in good agreement with previous measurements on internally finned monoliths,[11] indicating that in both cases similar flow phenomena are apparent, that is, film flow in the corners.

The reduced RTD curves deviate considerably between model and experiment, assuming uniform liquid distribution. A significant amount of liquid leaves the monolith earlier than predicted, indicated by earlier breakthrough times and lower peak values. At this point in time it is believed that maldistribution effects over the channel corners as well as over the channels themselves can explain a major part of the differences. Indeed the combination of a measured liquid distribution pattern in the channel corners and the fundamental convection–diffusion model resulted in a reduced distribution function very similar to the one determined from the experiments. Residual differences between model predictions and experiments might result from the occurrence of interfacial waves.

Future work will focus on the evaluation of size and shape effects of the monolith channels as well as the stacking of multiple monolith segments.

Acknowledgments

The help of Richard van Herk, during his graduation project at the TU Delft performing many of the RTD experiments, is greatly appreciated. Furthermore, Achim Heibel is grateful for the elaborate discussions concerning residence time distribution theory and experimental aspects with Dr. Shantanu Roy from Corning Inc.

Notation

A	area, m^2
Bo	Bodenstein number (ud_{char}/D)
c	concentration mg/mL
d	length dimension, m
D	diffusivity, m^2/s
E_t	residence time distribution function, 1/s
E_θ	reduced residence time distribution function
F_t	cumulative distribution function
F_θ	reduced cumulative distribution function
g	gravitational constant, m/s^2
I	intensity
k	constant Lambert–Beer law, mg/mL
l	length, m
S	surface area, m^2
t	time, s
u	velocity, m/s
V	volume, m^3
x	X-coordinate, mm
y	Y-coordinate, mm
z	axial channel coordinate, m

Greek letters

β	liquid saturation, m_L^3/m_V^3
ϕ	volume flow rate, m^3/s
η	dynamic viscosity, Pa·s
θ	reduced time
ρ	density, kg/m^3
σ_t	standard deviation, s
σ_θ	reduced standard deviation
τ	mean residence time, s

Subscripts

avg	average
ch	channel
char	characteristic
Coord	coordinate
e	exit
h	hydraulic
lat	lateral
L	liquid
loc	local
meas	measured
n	normalized
ref	reference
s	optical path length
s	superficial
V	void
λ	wavelength
θ	reduced time

Literature Cited

1. Heck RM, Farrauto RJ. *Catalytic Air Pollution Control—Commercial Technology*. New York, NY: Van Nostrand Reinhold; 1995.
2. Heck RM, Gulati S, Farrauto RJ. The application of monoliths for gas phase catalytic reactions. *Chemical Engineering Journal.* 2001;82: 149-156.
3. Kapteijn F, Nijhuis TA, Heiszwolf JJ, Moulijn JA. New non-traditional multiphase catalytic reactors based on monolithic structures. *Catalysis Today*. 2001;66:133-144.
4. Hatziantoniou V, Andersson B. The segmented two-phase flow monolithgic catalyst reactor. An alternative for liquid-phase hydrogenations. *Industrial & Engineering Chemistry Fundamentals*. 1984;23:82-88.
5. Crynes LL, Cerro RL, Abraham MA. Monolith froth reactor: Development of a novel three-phase catalytic system. *AIChE Journal.* 1995; 41:337-345.
6. Cybulski A, Stankiewicz A, Edvinsson RK, Moulijn JA. Monolithic reactors for fine chemicals industries: A comparative analysis of a monolithic reactor and a mechanically agitated slurry reactor. *Chemical Engineering Science.* 1999;54:2351-2358.
7. Heiszwolf JJ, Engelvaart LB, van den Eijnden MG, Kreutzer MT, Kapteijn F, Moulijn JA. Hydrodynamic aspects of the monolith loop reactor. *Chemical Engineering Science.* 2001;56:805-812.
8. Machado RM, Parrillo DJ, Boehme RP, Broekhuis RR. *Use of a Monolith Catalyst for the Hydrogenation of Dinitrotoluene to Toluenediamine*. U.S. Patent 6 005 143; 1999.
9. Edvinsson RK, Cybulski A. A comparison between the monolithic reactor and the trickle bed reactor for liquid phase hydrogenations. *Catalysis Today*. 1995;24:173-179.
10. Smits HA, Moulijn JA, Glasz WC, Stankiewicz A. Selective hydrogenation of styrene/1-octene mixtures over a monolith Pd catalyst. *Reaction Kinetics and Catalysis Letters*. 1997;60:351-356.
11. Lebens PJM. *Development and Design of a Monolith Reactor for Gas–Liquid Countercurrent Operation*. PhD Thesis. Delft, The Netherlands: Technical University of Delft; 1999.
12. Sie ST, Lebens PJM. Monolithic reactor for countercurrent gas–liquid

operation. In: Cybulski A, Moulijn JA, eds. *Structured Reactors and Catalysts*, Chemical Industries series. Vol. 71. New York, NY: Marcel Dekker; 1998:305-322.
13. Nijhuis TA, Beers AEW, Kapteijn F, Moulijn JA. Water removal by reactive stripping for solid-acid catalyzed esterification in a monolith reactor. *Chemical Engineering Science*. 2002;57:1627-1632.
14. Van Hasselt BW, Lebens PJM, Calis HPA, Kapteijn F, Sie ST, Moulijn JA. A numerical comparison of alternative three-phase reactors with a conventional trickle bed reactor. The advantage of countercurrent flow for hydrodesulfurization. *Chemical Engineering Science.* 1999;54:4791-4799.
15. Reilly JW, Sze M, Saranto U, Schmidt U. Aromatic reduction process is commercialized. *Oil and Gas Journal*. 1973;66-68.
16. Trambouze P. Countercurrent two-phase flow fixed bed catalytic reactors. *Chemical Engineering Science.* 1990;45:2269-2275.
17. Levenspiel O. *Chemical Reaction Engineering*. 3rd ed. New York, NY: Wiley; 1999.
18. Ramachandran PA, Chaudhari RV. *Three-Phase Catalytic Reactors*. 2nd ed. Philadelphia, PA: Gordon & Breach Science Publishers; 1992.
19. Platzer B, Steffani K, Grobe S. Möglichkeiten zur Vorausberechnung von Verweilzeitverteilungen. *Chemie Ingenieur Technik*. 1999;71: 795-807.
20. Chander A, Kundu A, Bej SK, Dalai AK, Vohra DK. Hydrodynamic characteristics of cocurrent upflow and downflow of gas and liquid in a fixed bed reactor. *Fuel*. 2001;80:1043-1053.
21. Iliuta I, Larachi F, Grandjean BPA. Residence time, mass transfer and back-mixing of the liquid in trickle flow reactors containing porous particles. *Chemical Engineering Science*. 1999;54:4099-4109.
22. Nigam KDP, Iliuta I, Larachi F. Liquid back-mixing and mass-transfer effects in trickle-bed reactors filled with porous catalyst particles. *Chemical Engineering and Processing*. 2002;41:365-371.
23. Van Swaaij WPM, Charpentier JC, Villermaux J. Residence time distribution in the liquid phase of trickle flow in packed columns. *Chemical Engineering Science.* 1969;24:1083-1095.
24. Götze L, Bailer O, von Scala C. Reactive distillation with KATAPAK. *Catalysis Today*. 2001;69:201-208.
25. Macías-Salinas R, Fair JR. Axial mixing in modern packings, gas, and liquid pases: II. Two-phase flow. *AIChE Journal.* 2000;46:79-91.
26. van Baten JM, Ellenberger J, Krishna R. Radial and axial dispersion of the liquid phase within a KATAPAK-S structure: Experiments vs. CFD simulations. *Chemical Engineering Science.* 2001;56:813-821.
27. Patrick RH, Klindera T, Crynes LL, Cerro RL, Abraham MA. Residence time distribution in three-phase monolith reactor. *AIChE Journal.* 1995;41:649-657.
28. Thulasidas TC, Abraham MA, Cerro RL. Dispersion during bubble-train flow in capillaries. *Chemical Engineering Science.* 1999;54:61-76.
29. Thulasidas TC, Cerro RL, Abraham MA. The monolith froth reactor: Residence time modelling and analysis. *Transactions of the Institution of Chemical Engineers*. 1995;73:314-319.
30. Lebens PJM, Stork MM, Kapteijn F, Sie ST, Moulijn JA. Hydrodynamics and mass transfer issues in a countercurrent gas–liquid internally finned monolith reactor. *Chemical Engineering Science*. 1999; 54:2381-2389.
31. Heibel AK, Scheenen TWJ, Heiszwolf JJ, VanAs H, Kapteijn F, Moulijn JA. Gas and liquid phase distribution and their effect on reactor performance in the monolith film flow reactor. *Chemical Engineering Science.* 2001;56:5935-5944.
32. Janssen LPBM, Warmoeskerken MMCG. *Transport Phenomena Data Companion*. Delft, The Netherlands: Delft University Press; 1991.
33. Comsol AB. FEMLAB software. Version 2.1. Stockholm, Sweden; 2001.
34. Fluent USA. *Fluent.* Version 6.0. Lebanon, NH; 2002.
35. Gupta P, Al-Dahhan MH, Dudukovic MP, Mills PL. A novel signal filtering methodology for obtaining liquid phase tracer responses from conductivity probes. *Flow Measurement and Instrumentation.* 2000; 11:123-131.
36. Pinheiro Torres A, Oliveira FAR. Residence time distribution studies in continuous thermal processing of liquid foods: A review. *Journal of Food Engineering*. 1998;36:1-30.
37. Mills PL, Dudukovic MP. Convolution and deconvolution of nonideal tracer response data with application to three-phase packed-beds. *Computers & Chemical Engineering*. 1989;13:881-898.
38. Heibel AK, Vergeldt FJ, Kapteijn F, Boger T, VanAs H, Moulijn JA. Gas and liquid distribution in the monolith film flow reactor. *AIChE Journal*. 2003;12:3007-3017.
39. Heibel AK, Heiszwolf JJ, Kapteijn F, Moulijn JA. Influence of channel geometry on hydrodynamics and mass transfer in the monolith film flow reactor. *Catalysis Today*. 2001;69:153-163.
40. Levenspiel O. *Chemical Reaction Engineering*. 3rd ed. New York, NY: Wiley; 1999.
41. SPSS Inc. *TableCurve® 2D User's Manual*. Version 4. Chicago, IL; 1996.
42. Heibel AK, Vergeldt FJ, Kapteijn F, Boger T, VanAs H, Moulijn JA. Gas and liquid distribution in the film flow monolith reactor. *AIChE Journal.* 2003;49:3007-3017.
43. Dao EK, Balakotaiah V. Experimental study of wave occlusion on falling films in a vertical pipe. *AIChE Journal.* 2000;46:1300-1306.
44. Fenwick DH, Blunt MJ. Three-dimensional modeling of three phase imbibition and drainage. *Advances in Water Resources*. 1997;21:121-143.
45. Kolb WB. *The Coating of Monolithic Structures: Analysis of Flow Phenomena*. PhD Thesis. Tulsa, OK: The University of Tulsa; 1993.
46. Lenormand R, Zarcone C, Sarr A. Mechanisms of the displacement of one fluid by another in a network of capillary ducts. *Journal of Fluid Mechanics*. 1983;135:337-353.
47. Ma S, Mason G, Morrow NR. Effect of contact angle on drainage and imbibition in regular polygonal tubes. *Colloids and Surfaces A: Physicochemical and Engineering Aspects*. 1996;117:273-291.

Manuscript received Dec. 8, 2003, and revision received May 5, 2004.